Supplemental Materials

1. Details of the DFT Setup

The density functional theory DFT is set up for self-consistent field calculations with an energy convergence criterion of 1×10^{-6} *eV/atom*. The Monkhorst-Pack method is used to sample points in the Brillouin zone, and the structural relaxation and static calculations are performed using a k-point mesh of 3×3×3. The k-point sampling distance is set to 0.03 A^{-1}, and the number of empty bands is three times the number of valence bands to ensure convergence of the refractive indices and octave coefficients.

2. Details of the MD Setup

The molecular dynamics simulation was carried out in the LAMMPS program and energy minimization was performed first to obtain the optimized structure. Subsequently, the NVT ensemble was first used to stabilize the temperature of the system at 310 K, then the NPT ensemble was selected to stabilize the pressure of the system at 1 atm, and finally the NVT ensemble was used to equilibrate the system at 310 K. The amorphous structure of the structure with complete chirp was obtained. This equilibrated conformation is used as the starting structure for subsequent material property calculations. Periodic boundary conditions were used throughout the simulation. Throughout the simulations, The L-J cut-off was set to 10Å and the Coulomb cut-off was set to 12Å . The simulation time step is 1 *fs*. The molecular force field is the CVFF force field, which provides a more accurate description of the structure and properties of the condensed state over a wide range.

3. Scattering-Absorption Model Setup Details

The PML is an artificial absorption layer used in numerical methods to truncate the computational domain to model open boundary problems. In this layer, electromagnetic waves are completely absorbed to avoid their return as reflections. This sets one of the boundary conditions for solving the model. In contrast, the scattering boundary marks the boundary of the space in which the medium and particles are located and defines the region in which the light extinction is calculated.

To solve the scattered field model, the background plane wave is set to propagate in the positive

direction along the y-axis and the electric field is polarized along the z-axis. The default boundary condition is a perfect electrical conductor applied to all external boundaries, including those perpendicular to the direction of polarization of the background electric field. The PEC (Perfect Electrical Conductor) symmetry plane is placed on the boundary perpendicular to the background E-field, and the Perfect Magnetic Conductor PMC (Perfect Magnetic Conductor) is placed on the boundary in the parallel direction. Therefore, the symmetry plane requires the addition of a perfect electric conductor PEC plane and a perfect magnetic conductor PMC plane. Where the X-Y plane is defined as the PEC plane and the Y-Z plane is defined as the PMC plane.

In the next step, the physical field was set up for the study. The model entailed solving for a fluctuating electromagnetic field, so a background electric field (E_0) was added. It was defined as moving in the y-direction, so the electric field was polarised along the z-axis, which is the longest axis of the particle. The polarisation of the particle is different when its position relative to the electric field changes. The electric field is defined by equation (S1).

$$E_0 = \sqrt{\frac{2I}{c \cdot \varepsilon_0 \cdot \sqrt{\varepsilon_{\text{rav}}}}} \tag{S1}$$

where c is the speed of light, $\varepsilon 0$ is the vacuum permittivity, and εrav is the average relative permittivity of the selected material. In order to direct the wave in the negative y-axis direction, the Eb vector is set to (S2).

$$E_b = E_0^{-i\kappa y} \tag{S2}$$

where κ is the wave propagation constant of the material.

The model is fine-meshed for the AuNP and PDA regions with a maximum cell size of 42.5 nm, a minimum cell size of 0.425 nm, a growth rate of 1.3, and a curvature factor of 0.2. The maximum size of the rest of the organized solution domain is set to 117 nm, the minimum cell size is set to 8.5 nm, the maximum cell growth rate is set to 1.4, and the curvature factor is set to 0.4. Appendix Figure S1 shows the mesh quality distribution, the closer the value is to 1 (the redder the color) represents the better the mesh quality, as can be seen from the figure, the vast majority of the small mesh quality is 1.

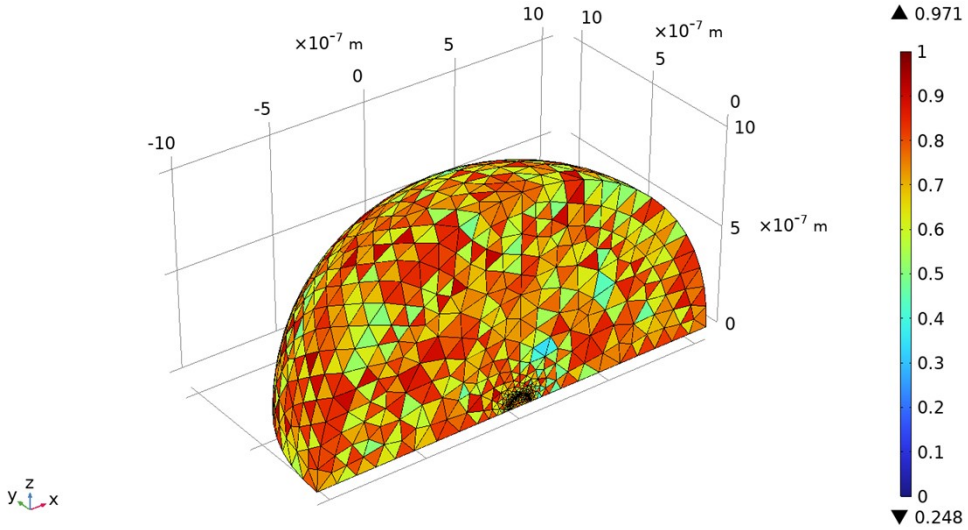

Figure S1 The mesh distribution of the scattering-absorption model.

4. Detail of tumor tissue photothermal therapy model

The tumor tissue region is finely meshed, with the maximum cell size set to 0.51 mm, the minimum cell size to 0.0051, the growth rate to 1.3, and the curvature factor to 0.2. The maximum size of the rest of the tissue solution domain is set to 1.4 mm, the minimum cell size to 0.102 mm, the maximum cell growth rate to 1.4, and the curvature factor to 0.4. Figure S2 shows the mesh quality distribution graph, the closer the value is to 1 (the redder the color is) represents the better quality of meshing, from the figure it can be seen that the mesh quality of the tumor region is almost 1.

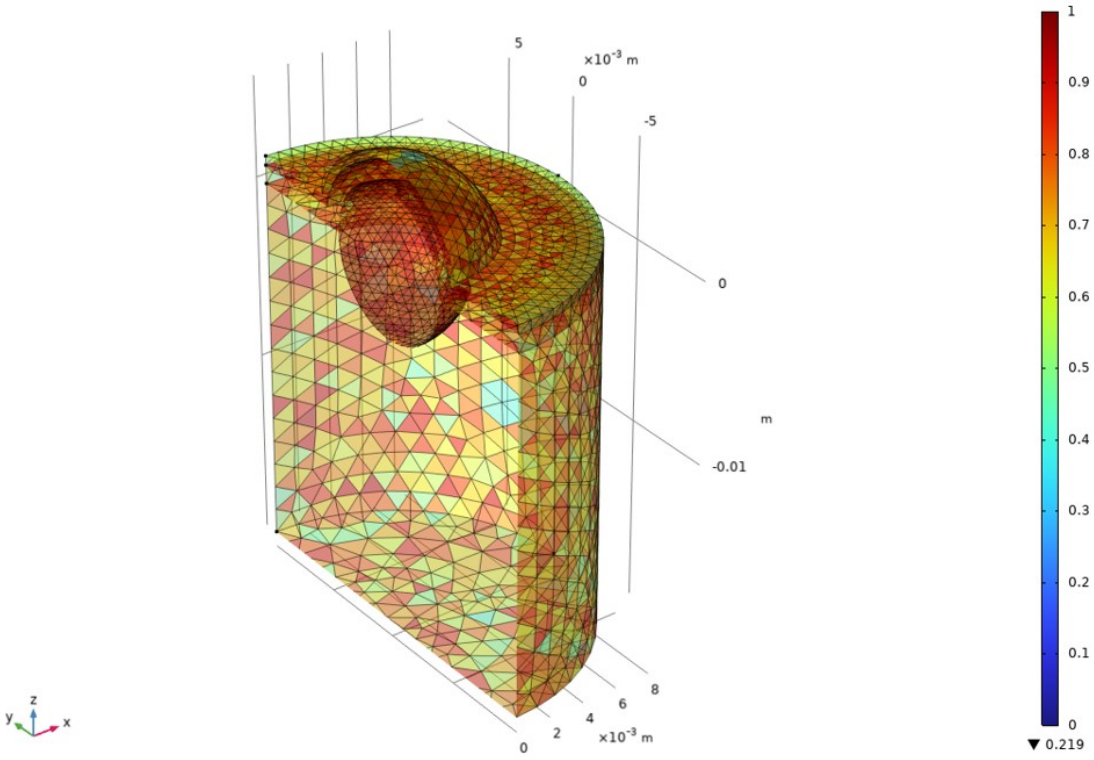

Figure S2 Multi-Organizational Model Grid Quality Distribution

As a miniature source of thermal energy within tumors, gold nanoparticles can achieve high absorption while maintaining a low scattering coefficient, i.e., effective absorption at relatively low irradiance levels [1]. In absorption-dominated media, incident light propagation is absorbed before it is significantly affected by scattering, and taking this into account, the Beer-Lambert law is used to calculate light absorption. Light intensity simulation using the Beer-Lambert law. For light intensity, this law can be written in differential form：

$$\frac{\partial I}{\partial z} = \alpha(T) I \tag{S1}$$

where I is the light intensity, z is the coordinate along the beam direction, and $\alpha(T)$ is the temperature dependent absorption coefficient of the material. Since the temperature varies with space and time, a controlled partial differential equation must be solved for the temperature distribution within the material:

$$\rho C_P \frac{\partial T}{\partial t} - \nabla \cdot (k \nabla T) = Q = \alpha(T) I \tag{S2}$$

where the heat source term is equal to the absorbed light.

The classical Pennes biological heat transfer equation [2] has been widely used to model heat transfer problems in biological tissues. In the case of uniform distribution of heat generated by blood and metabolism, the equation can be expressed as:

$$\rho C_p \frac{\partial T}{\partial t} - \nabla(k\nabla T) = \omega_b \rho_b C_{pb}(T_b - T) + Q_{met} \tag{S3}$$

Where the first term on the left is the heat conduction term, the second term is the general heat conduction term, and the first term on the right is the blood perfusion term. Where, ρ represents the tissue density, Cp represents the specific heat capacity of biological tissues, T represents the temperature of tissues, k represents the thermal conductivity of tissues, ω_b represents the blood perfusion rate of biological tissues, ρ_b represents the density of blood, Cp_b represents the specific heat capacity of blood, T_b represents the temperature of blood, Q_{met} represents the metabolic heat production rate of tissues, and t represents the calculation time.

Although the Pennes equation invokes the blood perfusion term to simplify the analysis and solution of the biological tissue heat transfer problem, its flexible application can solve most of the biological heat transfer problems, and it has become a widely used biological heat transfer model in biomedical fields at home and abroad.

In order to better describe the ablation of the tumor and the damage of the healthy tissue, the Arrhenius model was applied to analyze the thermal damage of the tissue, which is expressed as follows [3]:

$$\Omega(t) = \int_0^t A e^{\frac{-Ea}{RT(t)}} dt \tag{S4}$$

where Ea and A are the activation energy and frequency factor, respectively. R is the gas constant, equal to 8.314 J/(mol·K), and T is the absolute temperature of the tissue. Ω is the rate of thermal damage. If Ω is greater than 1, the tissue is considered to be permanently damaged.

The Arrhenius damage integral defines thermal damage by the cumulative energy of the medium (biological tissue) over time[4]. Although this is a quantitative metric, it only represents permanent thermal damage to biological tissue. In particular, permanent thermal damage as determined by the

Arrhenius damage integral does not include cell biological apoptosis, which includes apoptosis, necrosis, and charring. Cell death can manifest itself in various forms such as apoptosis, necrosis, and autophagy.

5. Optical property results

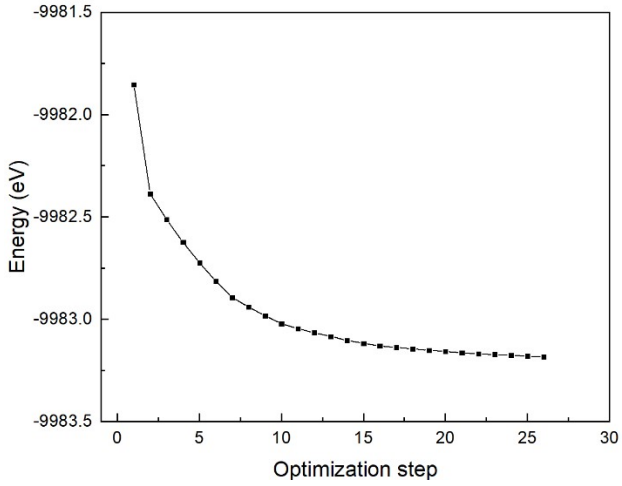

Figure S3 Total energy of PDA monomer

The real part ε1 and the imaginary part ε2 of the dielectric function of the PDA are shown in the Figure S4.

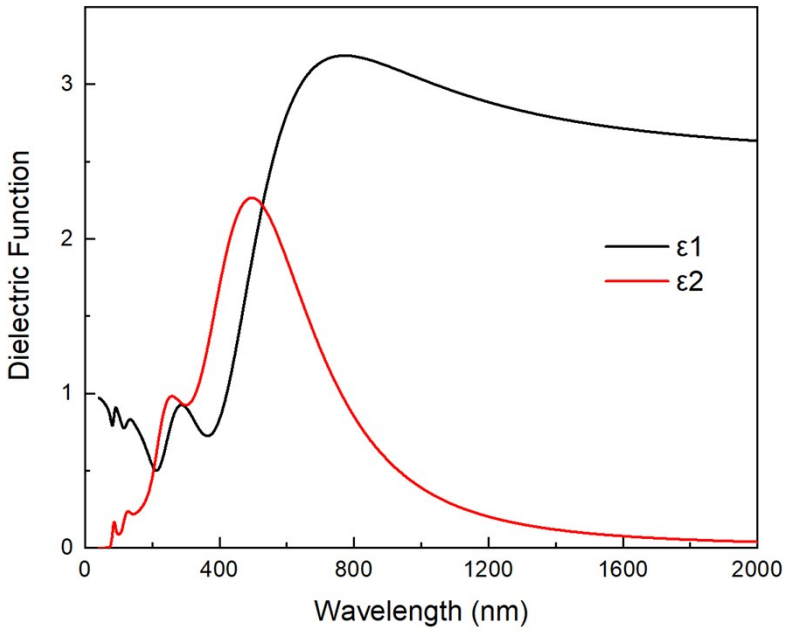

Figure S4 Dielectric function results

6. Structural analysis

The equilibrium structure of AuNP@PDA composite nanoparticles obtained from molecular dynamics simulations at 310 K temperature is shown in Figure S5.

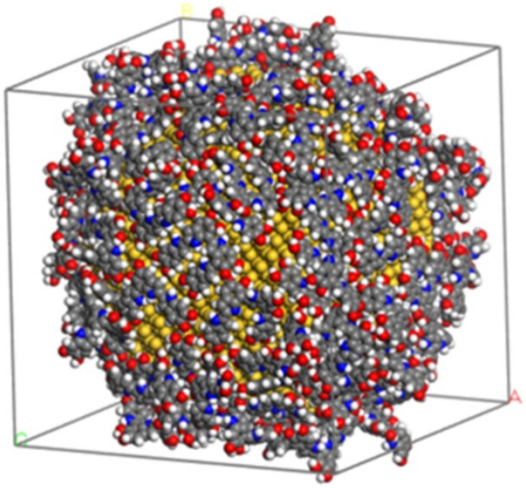

Figure S5 AuNP@PDA schematic diagram of the balanced structure

Table S1 lists the energies of the AuNP@PDA complex and the PDA system.

Table S1 Energy of AuNP@PDA and PDA

Energy (kcal/mol)	AuNP@PDA	PDA
Van der Waals effect	-355856.7	-2289.8
Electrostatic interaction	-9000.1	-8364.5
Kinetic energy	12988.5	6111.0
Potential energy	-328585.5	24743.5
Total energy	-315597.0	30854.6

The binding energy between PDA and AuNP was obtained by calculating the energy of each component of AuNP@PDA composite nanoparticles through Eqs. (S7).

$$E_{binding\ energy} = E_{Total} - (E_{AuNP} + E_{PDA}) \quad \text{(S7)}$$

Table S2 lists the binding energies of the AuNP@PDA complexes at 310 K temperature.

Table S2 Binding energy of AuNP@PDA

Energy (kcal/mol)	AuNP@PDA
PDA	30166.2

AuNP	-346846.6
Total energy	-328585.6
binding energy	-11905.2

The PDA-PDA and Au-Au radial distribution functions for the final equilibrium structure of the AuNP@PDA composites simulated by molecular dynamics at a temperature of 310 K are shown in Figure S6 (a) and (c), respectively, where Figure S6 (b) is the radial distribution function of Au-Au for the 6 nm bare AuNP, and Figure S6 (d) is the pure PDA system obtained by the same method for the radial distribution function of PDA-PDA. The Au-Au correlation function of AuNP, as shown in Figure S6 (b), shows several sharp and regular peaks within 20 Å, which corresponds to the periodically arranged Au atoms in AuNP. In contrast, the Au-Au correlation function of AuNP@PDA composite nanoparticles (Figure S6 (a)) has similar peak locations within 20 Å as bare AuNP, but with reduced sharpness and intensity. As shown in Figure S6 (d), the radial distribution function of pure PDA shows several characteristic correlation peaks only in the region below 5 A, apparently showing the amorphous structure characteristic of short-range order but long-range disorder. The location of correlation peaks in the radial distribution function (Figure S6 (c)) of PDA-PDA of AuNP@PDA composites is the same as that of the pure PDA system, but with a significantly higher intensity, indicating that the overall trend of PDA of the composites is similar to that of the pure PDA system, but the degree of polymerization is different, which is mainly due to the change of PDA molecules near the surface of AuNP, which makes the polymerization between PDAs more compact. The above results show that after the formation of AuNP@PDA nanocomposite system with PDA, the Au nanoparticles did not change the general characteristics of the periodic arrangement of their internal atoms, but the surface Au atomic layer was completely transformed into an amorphous state, and the periodicity of the internal Au atomic arrangement was decreased; the PDA still maintains an amorphous structure, but the polymerization between PDAs is more compact.

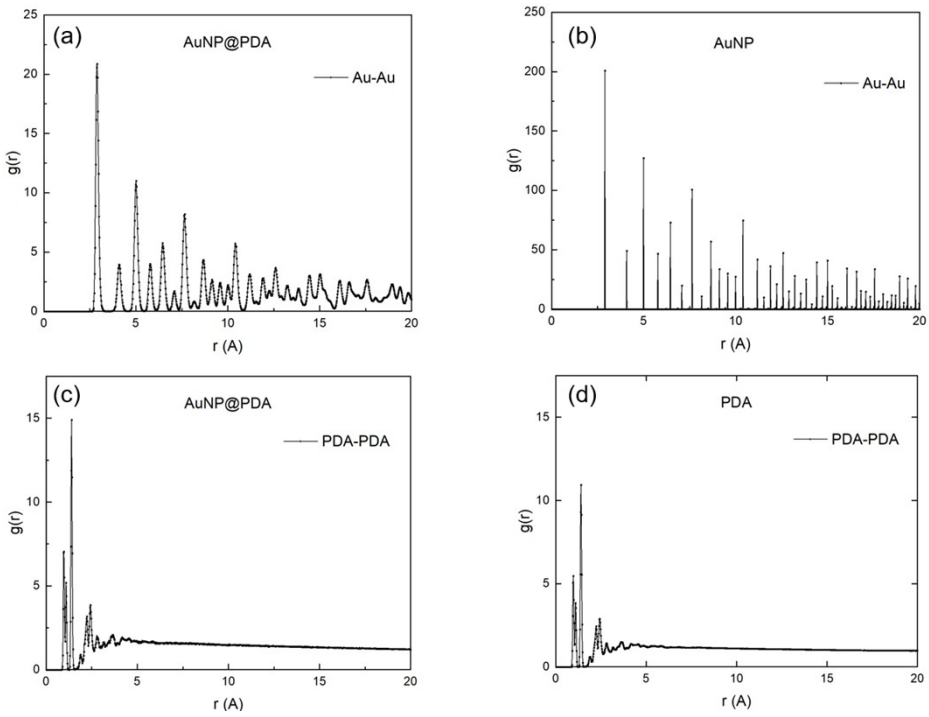

Figure S6 Radial distribution function plots. (a) Radial distribution function of Au-Au in AuNP@PDA; (b) Radial distribution function of Au-Au in AuNP; (c) Radial distribution function of PDA-PDA in AuNP@PDA; (d) Radial distribution function of PDA-PDA in PDA

In summary, AuNP is embedded in the polymer PDA to form a core-shell complex, with PDA acting as the shell layer material to impart better properties to the nanoparticles. The interfacial interactions between PDA and AuNP will provide a guide for model construction in the next finite element module.

7. Thermal conductivity

The Green-Kubo formula states that the transport coefficient is equal to the integral of the autocorrelation function over the correlation time. For the calculation of thermal conductivity there is the following Green-Kubo formula:

$$k_{\mu v}(t) = \frac{V}{k_B T^2}\int_0^t dt^{'} C_{\mu v}(t^{'}) \tag{S8}$$

where $k_{\mu v}(t)(\mu,v = x,y,z)$ is the thermal conductivity tensor, $t^{'}$ is the correlation time, k_B is the Boltzmann constant, T is the temperature, V is the volume, and $C_{\mu v}(t^{'})$ is the heat current

autocorrelation function.

The expression for the heat current autocorrelation function is given below:

$$C_{\mu v}(t) = \langle J_{\mu}(0) \cdot J_{v}(t) \rangle \tag{S9}$$

where J_{μ} (μ =x, y, z) is the heat flow. Since the system is studied isotropic (isotropic) in three dimensions, the final calculated thermal conductivity is taken as the average of the diagonal components:

$$k = \frac{k_{xx} + k_{yy} + k_{zz}}{3} \tag{S10}$$

Heat flow is defined as the time derivative of the energy density moment:

$$J = \frac{1}{V}\left[\sum_{i} e_i v_i - \sum_{i} S_i v_i\right] \tag{S11}$$

where e_i in the first term of the equation is the per-atom energy (potential and kinetic). This is calculated by the computes per-atom kinetic energy and per-atom potential energy. S_i in the second term is the per-atom stress tensor calculated by the compute per-atom stress. See compute stress/atom and compute centroid/stress/atom for possible definitions of atomic stress S_i in the case of bonded and many-body interactions. The tensor multiplies v_i by a 3×3 matrix to yield a vector. Note that as discussed below, the *I/V* scaling factor in the equation for *J* is not included in the calculation performed by these computes; you need to add it for a volume appropriate to the atoms included in the calculation.

8. Parameters

The model needs to obtain thermal and optical parameters for skin, fat, healthy tissue and breast tumor tissue. The tissue input parameters are shown in Table S3 .

Table S3 Thermal parameters of tissue

Parameters	Skin[5]	Fat[5]	Tumor[5]	Healthy Tissues[6]	Blood[6]	Unit

Density ρ	1180	1000	1150	1090	1060	Kg/m^3
Specific heat	2291	3148	4200	4181.3	3800	$J/(kg \cdot K)$
Thermal conductivity	0.58	0.58	0.561	1.1	-	$(W/(m \cdot K))$
Blood Perfusion	0.0005	0.00036	0.00036	0.00036	-	$1/s$
Metabolic heat production rate	420	420	420	420	-	W/m^3
Activating Energy	-	-	6.28×10^5	6.28×10^5	-	J/mol
Frequency Factor	-	-	3×10^{98}	3×10^{98}	-	$1/s$
Absorption Coefficient	19	6.5	6	3	-	$1/m$

Reference

1. Jacques, S. L., Role of tissue optics and pulse duration on tissue effects during high-power laser irradiation. *Appl Opt* **1993,** *32* (13), 2447-54.

2. Pennes, H. H., Analysis of tissue and arterial blood temperatures in the resting human forearm (Reprinted from Journal of Applied Physiology, vol 1, pg 93-122, 1948). *J Appl Physiol* **1998,** *85* (1), 5-34.

3. Diller, K. R.; Pearce, J. A., Issues in modeling thermal alterations in tissues. *Ann N Y Acad Sci* **1999,** *888*, 153-64.

4. Wright, N. T., On a relationship between the Arrhenius parameters from thermal damage studies. *J Biomech Eng-T Asme* **2003,** *125* (2), 300-304.

5. Xu, Y.; Long, S.; Yang, Y.; Zhou, F.; Dong, N.; Yan, K.; Wang, B.; Zeng, Y.; Du, N.; Li, X.; Chen, W. R., Mathematical simulation of temperature distribution in tumor tissue and surrounding healthy tissue treated by laser combined with indocyanine green. *Theor Biol Med Model* **2019,** *16* (1), 12.

6. Lee, S. S.; Oudjedi, F.; Kirk, A. G.; Paliouras, M.; Trifiro, M. A., Photothermal therapy of papillary thyroid cancer tumor xenografts with targeted thyroid stimulating hormone receptor antibody functionalized multiwalled carbon nanotubes. *Cancer Nanotechnology* **2023,** *14* (1).